Analysis of Dual Stator Winding Induction Generator-Based Wind Energy Conversion System Using Artificial Neural Network Maximum Power Point Tracking

N S D Prakash Korlepara*‡, E B Elanchezhian **, S Pragaspathy***

*Department of Electrical Engineering, Annamalai University, Chidambaram, India – 608 002

** Department of Electrical Engineering, FEAT, Annamalai University, Chidambaram, India – 608 002

***Electrical and Electronics Engineering, Vishnu Institute of Technology, Bhimavaram, Andhra Pradesh – 534 202

(prakash205k@gmail.com, elanchezhian.eb@gmail.com, pathyeee@yahoo.co.in)

‡ Corresponding Author: N S D Prakash Korlepara, Department of Electrical Engineering, Annamalai University, Chidambaram, India – 608 002, +91-8885720346, prakash205k@gmail.com

Received: 21.01.2022 Accepted: 22.02.2022

Abstract - This article proposes a switched Z source DC/DC converter based dual stator winding induction generator-based wind-energy-conversion-system (WECS) using an artificial neural network (ANN) maximum power point tracking (MPPT) control technique. Nowadays, multiphase machines are widely preferred for their increased power density, efficiency and improved reliability. In this article, a dual stator winding induction generator is proposed for WECS. A DC-DC converter plays a vital role in the peak power extraction and wide wind speed range operation of DSWIG in WECS. WECS is a high voltage and high-power application that necessitates high gain. A conventional boost converter may lead to an instability issue under a higher duty ratio for high gain. Hence, in this analysis, a switched Z-source DC/DC converter is proposed to avoid instability, which operates with a minimum duty ratio. The proposed topology utilises a backpropagation based neural network control approach to achieve the most accessible energy from the speed of the rotor and actual power. The results are compared with a classical power signal feedback method and an ANN-based MPPT with a boost DC-DC converter. Various topologies are analyzed in terms of voltage quality, power tracking, and tracking time using Matlab.

Keywords: Wind energy, dual stator winding induction generator, switched Z source DC/DC converter, MPPT, neural network, semiconductor excitation controller.

1. Introduction

In recent days, wind energy is becoming a popular and significant source of renewable energy. In many countries, it is preferred because it is cost-effective, clean and green energy [1,2]. Variable nature of wind speed influences the selection of generators in WECS and after many analysis researchers have reported that PMSG and doubly-fed induction generators (DFIG) are excellent choice of generators [3-7]. Compared to conventional three phase electric machines, polyphase machines offer enriched benefits. The advantages of multiphase machines are abundant power density and efficiency, finer precision and intrinsic fault tolerance [8-10]. A dual stator winding induction machine is a special category of polyphase winding induction machine with two individual windings in the stator and a brushless rotor. Vigorous and minimum maintenance are the foremost features of a squirrel cage induction generator, which makes it very appropriate for remote places (like offshore wind farms). In this article, DSWIM is presented for WECS. In 2009, Kai Shi et al. investigated WECS based on dual stator winding induction generators (DWIG) in a grid-connected mode for changing wind speed [11]. Kai Shi et al. (2016) used power-signal-feedback (PSF) MPPT to analyze a grid-connected DWIG wind power system over an extensive range of wind speeds [12]. Meryem Benakcha et al. (2017) investigated WECS based on twin

stator induction generators without the use of a DC-DC converter [13].

Tip speed ratio (TSR) MPPT is adopted to track maximum power in that analysis. Kamel Hamitouche et al., 2020 investigated dual stator winding induction generators (DSIG)-based standalone WECS under changing speed using TSR MPPT [14], For the DC load and battery, two three-phase IGBT converters are used. Juan I. Talpone et al., 2019 used TSR MPPT to investigate DWIG for WECS under varied wind profiles [15]. Two three-phase power converters are used in the system for AC-DC and DC-AC conversion.

Many researchers analysed DWIG for WECS without using a DC-DC converter, according to the survey. The large operating speed range of the generator in a wind power system is particularly useful for adopting broad wind speed changes and extracting wind power efficiently. The range of generator speed limits the strategies outlined above. Another control process must be used to change the DC voltage and alter the power flow. As a result, when the generator speed fluctuates, many transients arise. This can result oscillations in DC voltage and current, especially when there is little wind and a lot of turbulence. Hence to extract maximum power, a DC-DC converter is required to extend the DWIG speed range.

In article [16], Author proposed a new boost converter topology, which increases the DWIG generation speed range to 0.2-1.3 p.u and it is in corporate MPPT control system. In this study, a power speed curve look-up table (MPPT) is used. The entire survey states that many researchers analysed DWIG based WECS using PSFC and TSR MPPT alone. Yet, the calculations referenced above experience issues in assessing wind rate and speed of turbine in actual schemes and the framework's intricacy would increase when plotting the power-curve with no earlier information. The necessity of wind speed sensor increases cost of system, while PSFC necessitates accurate curve data for good tracking. Hence to overcome these drawbacks, an intelligent-control method of an artificial neural network is proposed in this analysis which evades the speed sensor and wind speed in MPPT methods. The soft computing dependent MPPT approaches namely neural network (NN) are meant for overcoming the disadvantages of controllers [17,18], NN offer quicker reaction significantly under sudden wind-speed fluctuations. For various conditions of speed of wind, the precision of soft computing dependent MPPT approach is great. A multilayer with one hidden layer is used to build the ANN technique. Through back propagation, network weights are being continuously adjusted throughout WECS operation with online training. As long as the required output is met, the control system will keep looking for the best method to get there [19]. So, in this article's peak power extraction, an ANN-based MPPT algorithm is provided.

The survey states that the simple boost converter is the only one examined by researchers in DWIG based WECS. The boost converter is generally employed in WECS for its simple structure and minimum expense [20]. Yet, the high-voltage nature of wind energy systems elevates the duty ratio, leading to instability. Hence, in this article, a switched Z-source DC-DC converter (SZSC) is put forward for acquiring high potential-gain along with a simplified topology and a low-duty ratio to avoid instability. In comparison to existing boost or Z-source converters, higher voltage gain is achieved with a low duty ratio (less than 25%), which avoids the instability caused by inductor saturation. Along with stability, proposed SZSC converter offers minimum losses, which supports in enhancing performance of WECS.

The efficiency of a WECS can be enhanced by minimising losses and obtaining the maximum amount of energy produced from each wind turbine. Hence in this paper both methods are proposed to enrich performance of DSWIG based WECS. In this article efficient MPPT method and effective SZSC DC-DC converter are proposed to extract maximum power with good voltage regulation over conventional boost and PSF MPPT method based DWIG-WECS.

2. Proposed DSWIG Based WECS

The proposed DSWIG based WECS is depicted in Figure 1. The proposed scheme has two converter control for control winding and power winding. Semiconductor Excitation Controller (SEC) is meant for controlling the converter linking with control winding. DC-DC converter with MPPT controller is linked with power winding which meets load/ grid.

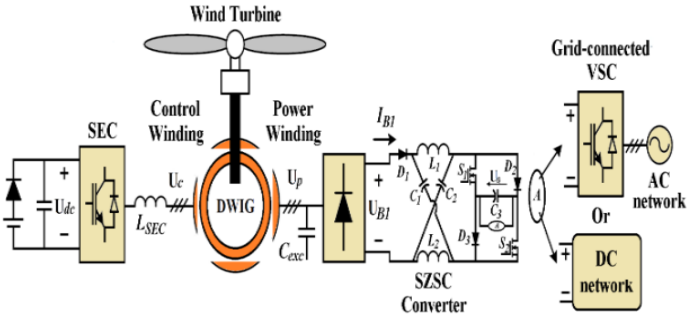

Fig.1. Proposed topology of DSWIG based WECS

The two windings in DSWIG are magnetically attached even it is electrically secluded. Some windings like power-winding windings are straightly attached to load. Rest of the winding is labeled as control-winding, which is fed from a Voltage-Source-Inverter (VSI) controlled using SEC and is utilized for maintaining the load voltage and frequency. A battery is employed as a real-energy storage shield; also charges capacitor, a diode in series with the battery gets reverse biased once capacitor voltage charges above the battery voltage. Meantime frequency is regulated depending upon the speed of generator and slip frequency forced by the load. Under low-speed condition, saturation due to low frequency is avoided by V/f control of SEC, which reduces the magnitude of voltage of control-winding.

Control and power winding voltage along with rotor voltage of DWIG in a d-q frame [21] are articulated as (1):

$$\begin{cases} u_{cd} = R_c i_{cd} - \omega\lambda_{cq} + \frac{d\lambda_{cd}}{dt} \\ u_{cq} = R_c i_{cq} + \omega\lambda_{cd} + \frac{d\lambda_{cq}}{dt} \\ u_{pd} = R_p i_{pd} - \omega\lambda_{pq} + \frac{d\lambda_{pd}}{dt} \\ u_{pq} = R_p i_{pq} + \omega\lambda_{pd} + \frac{d\lambda_{pq}}{dt} \\ u_{rd} = R_r i_{rd} - (\omega - \omega_r)\lambda_{rq} + \frac{d\lambda_{rd}}{dt} = 0 \\ u_{rq} = R_r i_{rq} + (\omega - \omega_r)\lambda_{rd} + \frac{d\lambda_{rq}}{dt} = 0 \end{cases} \quad (1)$$

where the angular synchronous frequency is ω and ω_r is the speed of rotor. Voltage, current and flux linkage are *u*, *i*, and λ. The parameters of control and power-winding, and rotor are represented with the indices of *c*, *p*, and *r*. Mutually *c* and *r* constraints are moved to *p* side in the model. As a result of squirrel cage type rotor, the *r* voltage is zero for both d and q axis. In (2), the linkage fluxes calculations are expressed:

$$\begin{cases} \lambda_{cd} = L_c i_{cd} + L_{cp} i_{pd} + L_{cr} i_{rd} \\ \lambda_{cq} = L_c i_{cq} + L_{cp} i_{pq} + L_{cr} i_{rq} \\ \lambda_{pd} = L_{pc} i_{cd} + L_p i_{pd} + L_{pr} i_{rd} \\ \lambda_{pq} = L_{pc} i_{cq} + L_p i_{pq} + L_{pr} i_{rq} \\ \lambda_{rd} = L_{rc} i_{cd} + L_{rp} i_{pd} + L_r i_{rd} \\ \lambda_{rq} = L_{rc} i_{cq} + L_{rp} i_{pq} + L_r i_{rq} \end{cases} \quad (2)$$

c and *p*, and rotor inductances are expressed in (3):

$$\begin{cases} L_c = L_{lc} + L_{lcp} + L_m \\ L_p = L_{lp} + L_{lcp} + L_m \\ L_r = L_{lr} + L_m \\ L_{cp} = L_{pc} = L_{lcp} + L_m \\ L_{cr} = L_{rc} = L_m \\ L_{pr} = L_{rp} = L_m \end{cases} \quad (3)$$

in which the L_{lc}, $L_{lp}$and L_{lr} are the leakage inductances of *c*, *p* and *r*, and magnetizing inductance is referred to as L_m. The mutual leakage inductance amid *c* and *p* (L_{lcp}) is ignored by reason of its insignificant value.

3. DWIG Excitation Control Strategy

The *c*-voltage (U_c) adjustment is the primary thing of SEC for exciting DWIG, as the boost converter is utilised for increasing the output voltage level in the presented topology, for a low-speed generation, the *V/f* approach is employed in DWIG excitation controller. Hence, the DC link voltage of SEC (U_{dc}) should be controlled at a base value. So as for adjusting the U_c and U_{dc}, in this article, the CWVO technique is proposed. The illustration of CWVO control technique for DWIG is showed in Fig 2.

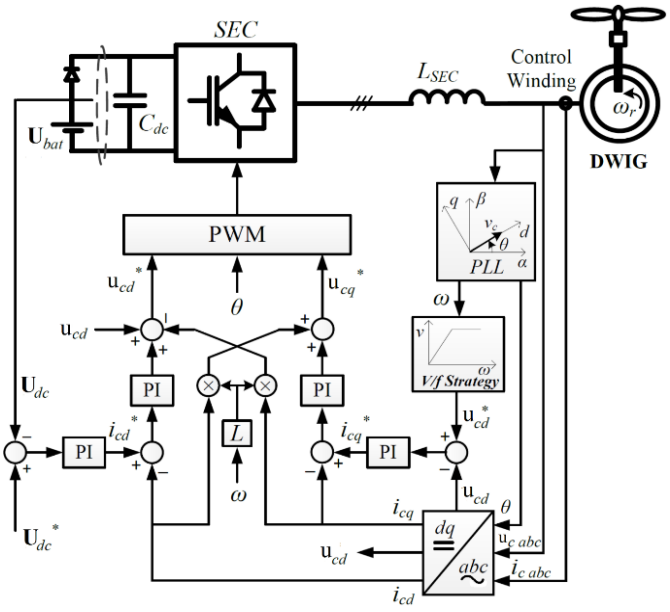

Fig. 2. DWIG CWVO excitation control strategy

In this technique, line up the control-winding voltage by means of d-axis, the q-axis voltage (u_{cq}) turns to zero whereas the voltage of d-axis (u_{cd}) same as the magnitude of U_c as expressed below [22]:

$$\begin{cases} u_{cd} = |U_c| \\ u_{cq} = 0 \end{cases} \quad (4)$$

Consequently, in line with instantaneous power theory, the active and reactive power of control winding i.e. (p_c) and (q_c) are:

$$\begin{cases} p_c = \frac{3}{2} u_{cd} i_{cd} \\ q_c = -\frac{3}{2} u_{cd} i_{cq} \end{cases} \quad (5)$$

For u_{cd} in (1), if the potential drop across the winding resistance ($R_c i_{cd}$) is ignored and the *c* d-axis flux is made as constant$\left(\frac{d\lambda_{cd}}{dt} = 0\right)$, then:

$$u_{cd} \simeq -\omega\lambda_{cq} \quad (6)$$

and (5) is altered as:

$$\begin{cases} p_c \simeq -\frac{3}{2} \omega\lambda_{cq} i_{cd} \\ q_c \simeq +\frac{3}{2} \omega\lambda_{cq} i_{cq} \end{cases} \quad (7)$$

The above equation depicts that by i_{cd} andi_{cq}, the p_c and q_c are controlled.

In (8), the power equilibrium amid *c* and U_{dc} is articulated:

$$\frac{\partial\left(\frac{1}{2} C_{dc} U_{dc}^2\right)}{\partial t} + p_{SEC\_loss} = -p_c \quad (8)$$

In equation (8) SEC DC link capacitor is C_{dc} and the power loss is $p_{SEC\ loss}$. Like a Static Synchronous Compensator (STATCOM), while swapping reactive power,

the SEC consumes small active power for its internal $p_{SEC\ loss}$; for maintaining the DC link voltage as steady. So, the U_{dc} regulated by p_c.

As portrayed in, at various speeds, the control-winding flux (λ_{cq}) is regulated with control-winding reactive power (q_c) [23]. This is expressed by (9) with the help of expressions (2) and (7):

$$\lambda_{cq} \cdot \lambda_{ccq} = q_c \cdot L_s / \omega \tag{9}$$

where a part of the λ_{cq} is λ_{ccq}, which persuaded by i_{sq}in *c*. Therefore, the magnitude of U_c is controlled by regulating the λ_{cq} as expressed by (4) and (6). Therefore, (7), (8), and (9) taking into consideration and articulated that:

$$\begin{cases} i_{cd} \Rightarrow p_c \Rightarrow U_{dc} \\ i_{cq} \Rightarrow q_c \Rightarrow \lambda_{cq} \Rightarrow U_c \end{cases} \tag{10}$$

In this system, the regulation of U_{dc} and voltage of control winding (U_c) is performed by the control of i_{cd} and i_{cq} as showed in equation (10). In DWIG excitation control approach, as illustrated in Figure 2, the controller utilises a decoupling approach using proportional integral (PI) controllers in a current circle for controlling i_{cd} and i_{cq} distinctly and not based on parameters of DWIG [24]. For determining the reference current of control-winding in d-axis (i_{cd}^*), the difference amid U_{dc} and its reference is deal with by the PI controller. Likewise, the difference amid U_{cd} and its reference is deal with by another PI controller to get q-axis reference current (i_{cq}^*). *V/f* approach is applied at low frequency conditions, as per the less generator speed, i.e. $U_{sd}^*$is known as per the operating frequency.

4. Power Winding Control Strategy

By using MPPT, the power winding control circuit controls the active power of DWIG, and the voltage is fine-tuned by excitation control. The DC-DC converter gives an extensive speed range of working, as well as in slighter-speed operations, where the potential of DWIG is abridged by *V/f* technique. DC-DC converter lifts the output voltage, makes the generator to a developed voltage level. The power winding control system relies on the DC-DC converter and technique of MPPT. Enhancement in WECS utilizing DWIG is analyzed in this article using enrichment in DC-DC converter in company with MPPT.

The MPPT method in the conventional system is power speed curve-based tracking, in this analysis which is enhanced by proposing artificial-neural-network based MPPT. Generally, a simple boost converter is employed in WECS to enrich DC-DC converter performance, which decides the quality of load/ grid voltage; in this work switched Z source converter is analyzed.

- Control strategy 1: Boost converter with power-signal feedback control MPPT
- Control strategy 2: Boost converter with ANN MPPT
- Control strategy 3: Switched Z source converter with ANN MPPT

4.1 Control Strategy 1: Boost Converter with Power Signal Feedback Control MPPT

Figure 3 depicts the control approach for the boost converter with PSFC MPPT.

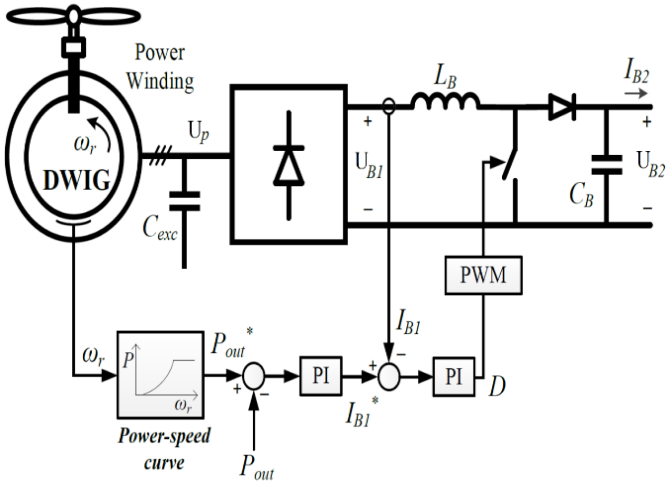

Fig. 3. The control strategy for the boost converter

Figure 3 illustrated the controller utilises a look-up table, is attained carried out by curves of power-speed for achieving MPPT. For at all speed (ω_r), the optimum power (P_{out}*) is logged in look-up table. For adjusting the output at MPP, in boost controller the P_{out}* is taken as base power. If the boost converter power loss is pass over, the output power (P_{out}) is acquired from (11):

$$P_{out} = U_{B2} I_{B2} \simeq U_{B1} I_{B1} \tag{11}$$

U_{B1} is marked as a constant ratio of voltage of *p* when the potential drop in diode rectifier is neglected. So, the U_p is supplanted by U_c considering the drop of voltage across the generator impedance. The drop of voltage relies upon the i_c and i_p acquire by rectifier/boost converter current and U_c. Difference between P_{out} and P_{out}* is deal by a PI controller in power regulation loop for obtaining the reference value of I_{B1} (I_{B1}*). The difference between I_{B1} and I_{B1}* is moved over another PI controller in current regulation loop for getting the boost converter duty cycle (*D*). At last, the duty cycle is converted to pulse by PWM strategy to switch drive.

4.2 Control Strategy 2: Boost Converter with ANN MPPT

The important and extensively utilised neural-network is the Feedforward neural-network. The backpropagation trained neural network (BPNN) by Levenberg–Marquardt (LM) approach is proposed in this article. In neural-network, the LM is a famous supervised learning technique [25]. The BPNN offers expected yield depending upon the input, method of training and weights. BPNN based MPPT control algorithm generates a reference power for attaining the peak power (P*) for system configuration at variable wind speeds. In this analysis, produced power and rotor speed are utilised to train the network.

The network is made with three layers. Input and output are border layers having middle layer as hidden layer. The input layer holds two-neurons for generated power and rotor speed. The hidden layer is formed through ten neurons, while the output layer is intended with neuron for P*. To train ANN, 9,55,594 samples are included for getting the accurate output in this research. ANN employed in WECS converges training with MSE of 3.1 X 10^{-8} in 2.75s with 112 epochs. This trained ANN is proposed as MPPT to enrich peak power tracking.

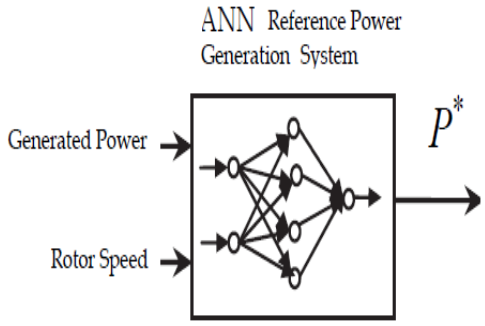

Fig. 4. ANN MPPT

4.3 Control Strategy 3: Switched Z Source Converter with ANN MPPT

The power-winding control system relies on the DC-DC converter; this analysis Switched Z source converter is presented. Figure 5 shows the proposed SZSC base power winding control circuit of DSWIG based WECS.

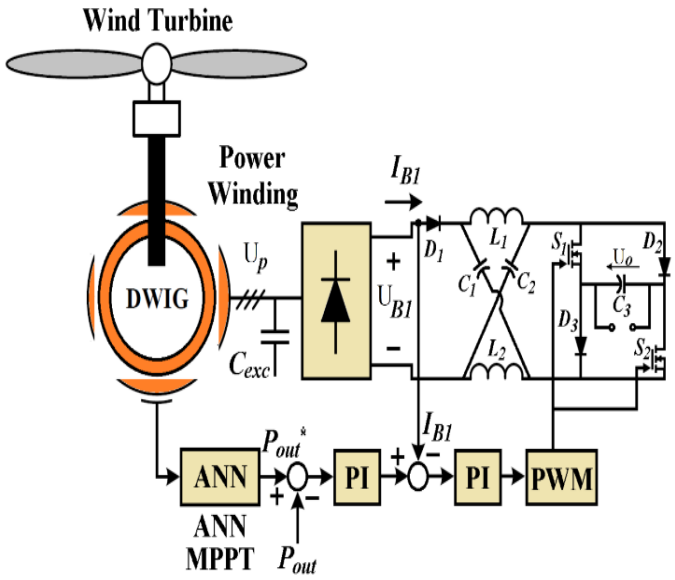

Fig. 5. Proposed SZSC base power winding control circuit of DSWIG based WECS

4.3.1 Configuration and Principle of Proposed SZSC

Figure 5 depicts the analysed SZSC circuit. First half of this converter is like conventional Z-source dc-dc converter. The converter's next half is contrarily comprised of couple of switches (S_1 and S_2) and diodes (D_2 and D_3) with an o/p capacitor (C_3). Additionally, S_2 and D_3 are introduced in contrast with the conventional one. C_3 is accompanied by the function of filtering, additionally charges the Z-network while both S_1 and S_2 are in on state. The minor variations result in increased voltage gain to $1/(1\text{-}4D)$, is like that of the complex hybrid three Z-source converters. Likewise, the D must be lower than 0.25, i.e., $0<D<0.25$, which evade the unsteadiness produced by saturation of the inductors [26].

4.3.2 Operating Principle of Proposed SZSC

Formerly, suppositions made are: entire power devices are ideal by considering nil on-state resistances or forward potential drops. The capacitors are adequate for negligible voltage ripples; the put forward SZSC functions in continuous current mode (CCM).

Both switches are turned on or off concurrently in the presented converter, states that both switches are triggered by the same gate signal, as illustrated in Figure 6. Concerning the switching states of S_1 and S_2, the entire period of proposed converter is separated into two modes, i.e., Mode I and Mode II, alike to conventional Z-source dc-dc converter as shown in figure 7 [27].

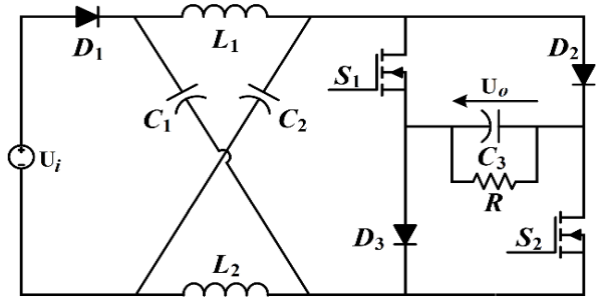

Fig. 6 Proposed SZSC circuit

Figure 8 illustrates the equivalent circuits of designed SZSC in both states, where u_{L1}, u_{L2}, U_{C1}, U_{C2}, and U_{C3} are the voltages over L_1, L_2, C_1, C_2, and C_3, correspondingly.

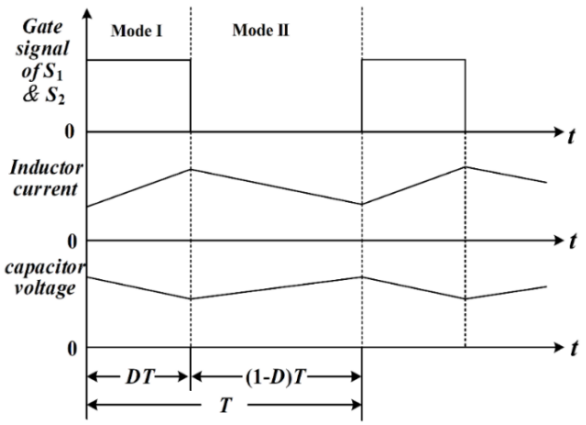

Fig. 7. Functional principles of the proposed SZSC

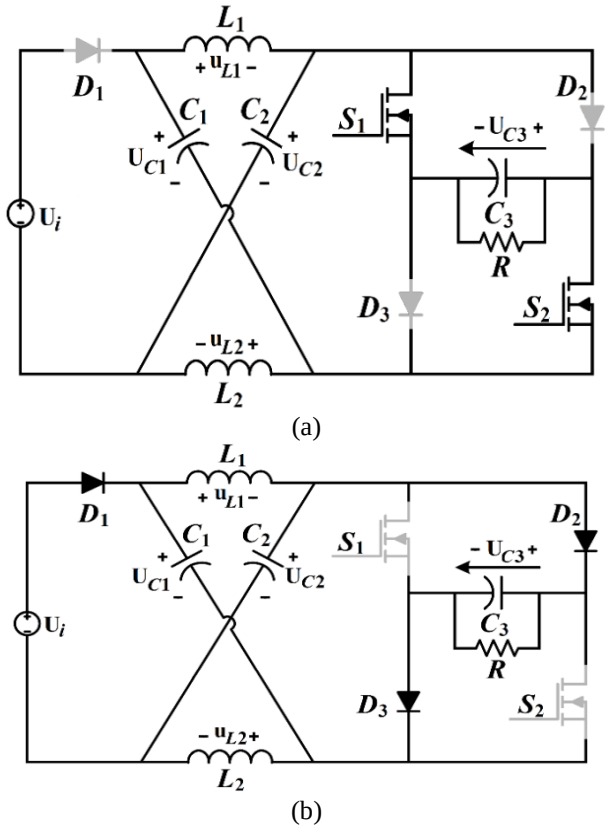

Fig.8. Equivalent circuits of the proposed SZSC (a) Mode I (b) Mode II

***Mode I [0, DT]*:** Both switches are turned on in this mode, and diodes D_1 -D_3 are all reversed biased, as illustrated in Figure 8(a). During this mode, series-connected capacitors C_1 and C_3 charge the inductor L_1 while the inductor L_2 is altered by the series-connected capacitors C_2 and C_3; capacitor C_3 supplies the load. As per Kirchhoff's voltage law (KVL), potential across the inductors in this mode and the output voltage U_o can be attained.

$$\begin{cases} u_{L1} = U_{C1} + U_{C3} \\ u_{L2} = U_{C2} + U_{C3} \\ U_o = U_{C3} \end{cases} \quad (12)$$

In view of the evenness of this SZSC, the subsequent equation occurs in an entire period, as

$$\begin{cases} u_{L1} = U_{L2} \\ u_{C1} = U_{C2} \end{cases} \quad (13)$$

***Mode II [DT, T]*:** Both switches are switched off in this mode and diodes D_1 - D_3 are all forward conducted, is showed in Figure 8(b). On this state, C_1 is charged by the U_i and L_2 while the C_2 is charged by the U_i and L_1; the U_i charges the C_3 and L_1 and L_2 supplies the load too. Likewise, as per KVL, the accompanying calculations are acquired.

$$\begin{cases} u_{L1} = U_i - U_{C2} \\ u_{L2} = U_i - U_{C1} \\ U_{C3} = U_{C1} + U_{C2} - U_i \end{cases} \quad (14)$$

In line with the volt-second management of both inductors, the constant variables in expressions (12)-(14) can be resolved as

$$\begin{cases} U_{C1} = U_{C2} = \frac{1-2D}{1-4D} U_i \\ U_o = U_{C3} = \frac{1}{1-4D} U_i \end{cases} \quad (15)$$

From (15), the proposed SZSC ideal voltage gain is 1/(1-4*D*), is alike to complex hybrid three Z-source DC-DC converters in but the number of passive components are abridged significantly [26,28].

Hence compared to boost converter by a low duty ratio, high-voltage gain is achieved. ANN MPPT receives produced power and speed of rotor as inputs to track maximum power and produces P*, which is processed as deliberated in control strategy 1 and produces reference signal to PWM. PWM generator controls both switches in SZSC. Switches S_1, S_2 are controlled by ANN MPPT to deliver maximum output with constant voltage.

5. Simulation Results and Analysis

The dual stator winding induction-generator based WECS performance is analysed using Matlab. Parameters of the DSWIG is shown in Table 1.

Table 1. Parameters of the DSWIG

Parameter	Value
Rated output power	5kW
Rated power winding line voltage	230V
Rated control winding line voltage	115V
Poles	2
Base frequency	50Hz
Base rotation speed	3000 rpm
Rated rotation speed	3600 rpm
Power winding resistance	0.304 Ω
Power winding leakage inductance	2.8mH
Control winding resistance	0.6 Ω
Control winding leakage inductance	2.9mH
Rotor resistance	0.326 Ω
Rotor leakage inductance	3.04mH
Magnetizing inductance	34mH

Proposed converter is designed as Fs=20kHz, L_1= L_2=10mH and C_2= C_2=100μF [28]. Three control approaches are analysed under a broad speed range. To analyse the performance of a proposed system, the rotor started with a speed of 0.4 p.u; after 1 second, it is slowly increased to 0.9 p.u at 2 seconds. The same speed is maintained till 3 seconds, after than it raised and reaches 1.2 p.u at the time of 4.5s, then kept at equivalent speed. The WECS using DSWIG under PSF MPPPT with boost converter performance is depicted in Figure 9.

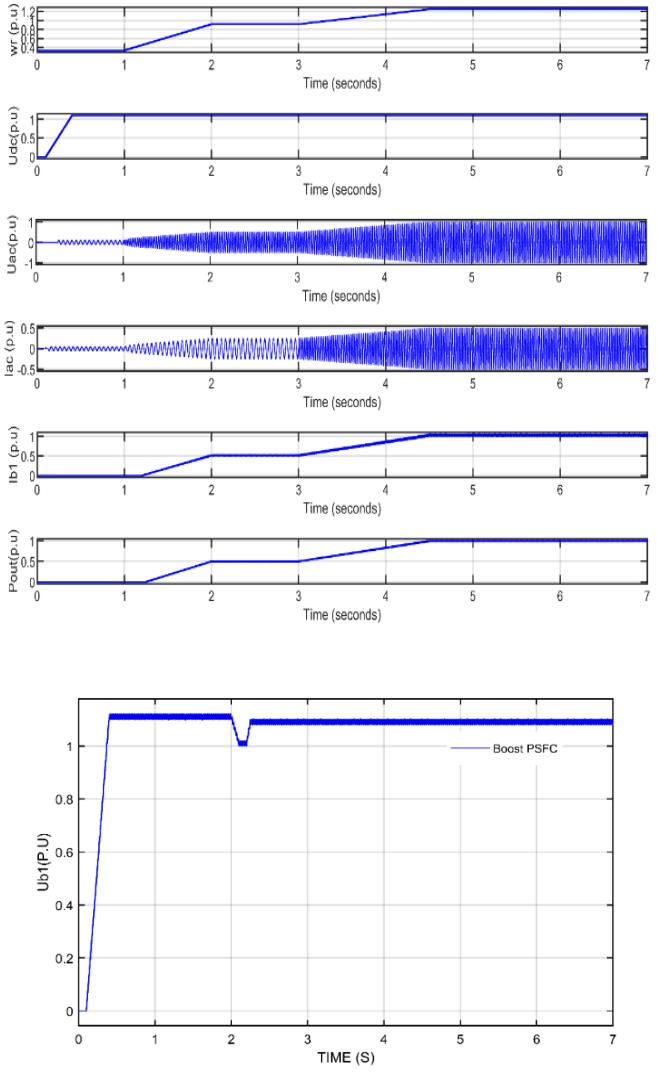

Fig.9. Performance of WECS using DSWIG under PSFC MPPPT with boost converter (a) Rotor speed (b) DC link voltage (c) Voltage (d) current (e) Power (g) DC bus voltage.

Initially, the rotor speed 0.4 p.u, as depicted in Figure 9(a). At 0.1s SEC controller is triggered and at 0.2s, the DC-link voltage of SEC (U_{dc}) and control-winding voltage begins to rise, as illustrated in Figure 9(b). At 0.4s, the DC-link voltage settles at 1.1 p.u. The voltage and current are also increased according to the rotor speed. At 2s, a drop in voltage in the power winding voltage (U_{B1}) from 1.1p.u to 1.0075 p.u due to rise in I_{B1}, then gradually raised and settled back to 1.0881 p.u. as depicted in Figure 9(g). After voltage of SEC accumulation, at any speeds, the current is restricted to 0.5 p.u., expresses the appropriateness of excitation capacitor election. In this analysis, current is limited to 0.5 p.u to attain maximum power with the help of the properness of excitation capacitor selection.

As the rotor speed increased gradually about 0.9p.u. at 3s, the I_{B1} and output power gets exponentially increased; after 4.5s, the speed of rotor is 1.2 p.u, at this time, the current ripple of I_{B1} is 0.04878% shown in Figure 9(e); the power tracked by the PSFC-BC is 0.99283 p.u and the tracking time is 0.14s illustrated in Figure 9(f). In startup progression, due to low-speed process, the voltage magnitude is restricted to 0.1 p.u. to evade DWIG magnetic saturation. From figure 9(b) and 9(g), it is observed that oscillation in the power winding voltage (U_{B1}) is regulated to U_{dc} with the help of boost converter with MPPT. Figure 10 depicts the performance of WECS using DSWIG under ANN MPPPT with boost converter.

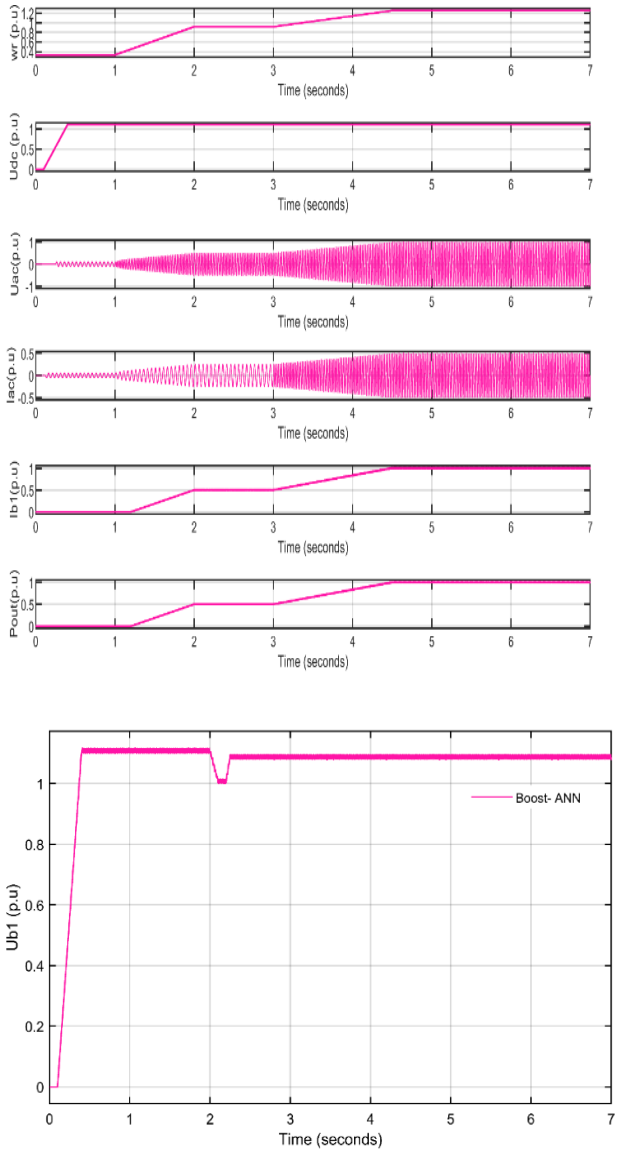

Fig. 10. Performance of WECS using DSWIG under ANN MPPPT with boost converter (a) Rotor speed (b) DC link voltage (c) Voltage (d) current (e) IB1 (f) Power (g) DC bus voltage.

Figure 10 illustrates the simulation result of the system with ANN-BC. Rotor speed, DC-link voltage, U_{B1} and V_{ac} performance of ANN MPPT is like PSF MPPT with a boost converter. ANN MPPT reduces the boost converter current ripple to 0.0201% as illustrated in Figure 10(e) while it is 0.04878% by PSFC MPPT. Output power injected to grid by ANN MPPT is 0.9999 p.u with a tracking time of 0.1s. Compared PSFC MPPT 0.00707 p.u of power tracked is increased through ANN MPPT. Meantime tracking time is also reduced from 0.14s to 0.1s by the ANN MPPT. From Figure 10, it is observed that, the output power is improved, and the current ripple is reduced with ANN-BC in contrast to PSFC-BC, as discussed before. Figure 10 illustrates the performance of WECS using DSWIG under ANN MPPPT with switched Z source converter.

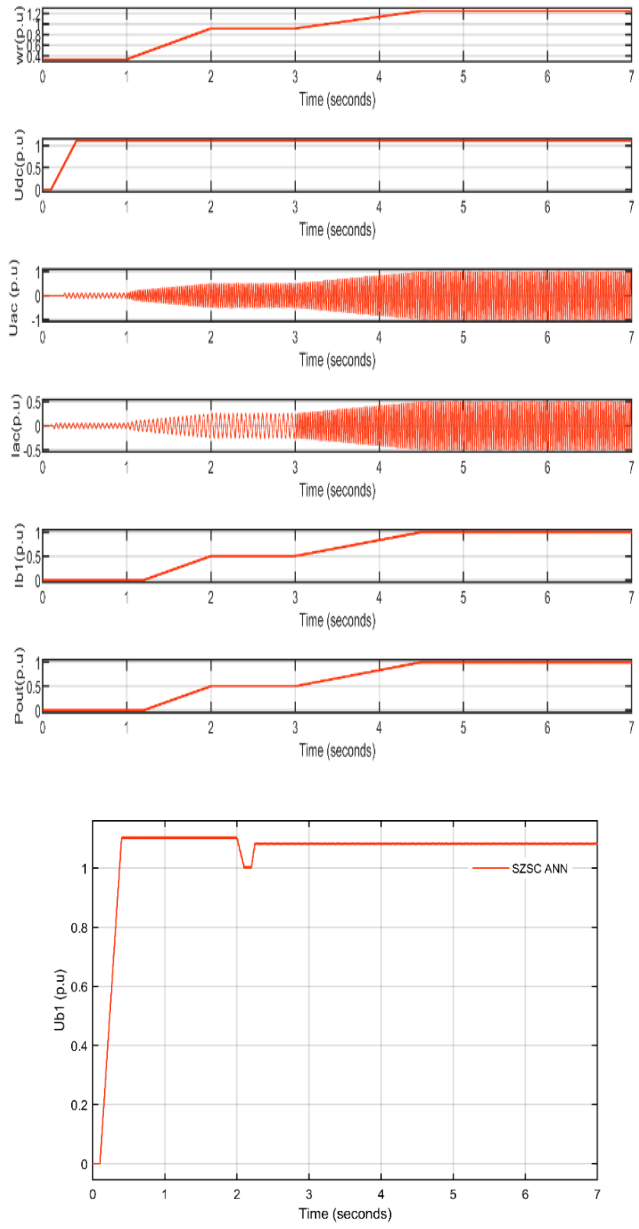

Fig. 11. Performance of WECS using DSWIG under ANN MPPPT with SZSC (a) Rotor speed (b) DC link voltage (c) Voltage (d) current (e) IB1 (f) Power (g) DC bus voltage.

Figure 11 shows the simulation result with ANN-SZSC. Rotor speed, DC-link voltage and Uac performance of ANN MPPT is same as the other two control strategies. ANN MPPT with SZSC tracks the peak power of 1 p.u with a tracking time of 0.1s, as depicted in Figure 11(f). Performance comparison of three control strategies is depicted in Table 2.

Table 2 Performance comparison of three control strategies

Control strategies	Maximum power tracked (P.U)	Power tracking time (s)	Current ripple (%)
Boost PSFC	0.99283	0.14	0.04878
Boost ANN	0.9999	0.1	0.0201
SZSC ANN	1.0	0.1	0.00995

From Table 2, it is observed that, the peak power tracked by proposed configuration is high compared to other two methods. Tracking time is reduced around 0.04s by proposed configuration compared to PSFC MPPT. ANN MPPT improves power tracked and reduces tracking time. Meantime the current ripple is reduced to 0.00995% by proposed configuration as depicted in Table1, while it is 0.0201% by ANN-BC and 0.04878% by PSFC-BC. Influence of converter shows an effective minimization in the current ripple compared to other strategies. It is seen that the ANN-SZSC has improved performance than the output power-driven by the PSFC-BC and ANN-BC along with minimum current ripple. The contrast of DC bus voltage under three control strategies such as PSFC-BC, ANN-BC, and ANN-SZSC is shown in Figure 12, Table 3 and Figure 13.

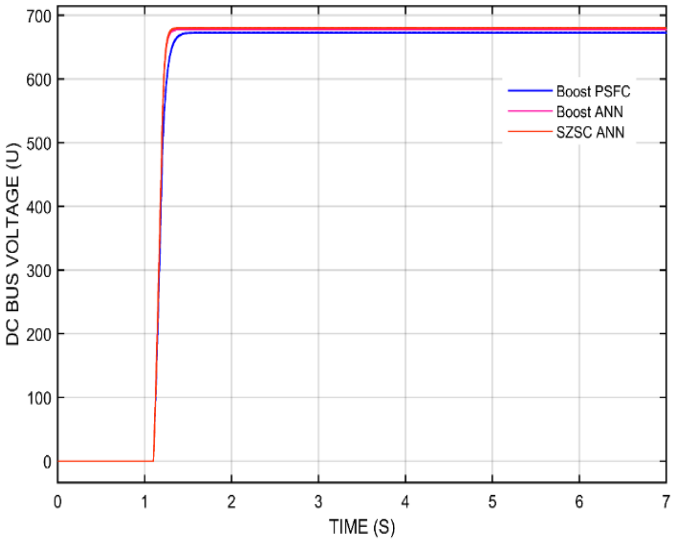

Fig.12. Comparison of DC bus voltage

According to Figure 12, the PSFC-BC settles the voltage to 672.75V in 1.15s. In the other two approaches, the influence of ANN MPPT reduces the settling time to 1.0s. The DC bus voltage generated by ANN-BC is 677.54V, which is higher than the voltage generated by PSFC MPPT. The fact that ANN-SZSC maintains the DC bus voltage at 680.22V, which is significantly higher than the other two approaches, demonstrates the proposed SZSC converter's effectiveness.

Table 3 Comparison of DC bus voltage under three control strategies

Control strategies	Settling time (s)	Ripple ratio (%)	Steady-state error (%)
Boost PSFC	1.15	0.074	1.21
Boost ANN	1.0	0.017	0.51
SZSC ANN	1.0	0.0059	-0.11

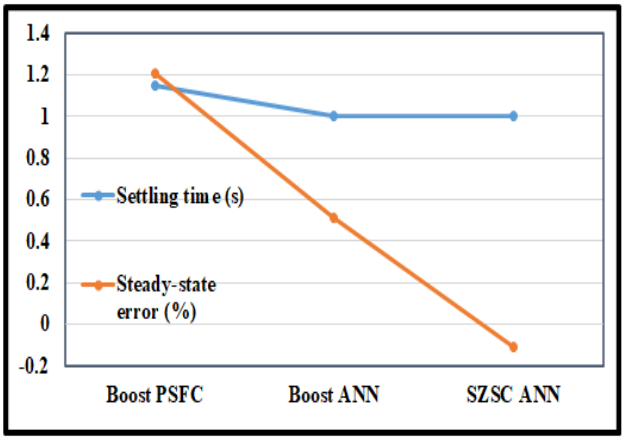

Figure 13 Comparative performance of DC bus voltage

Comparative performance of DC bus voltage is observed from Table 3 and Figure 13. In Table 3, Steady state error is calculated by percentage of error in settled voltage with respect to reference voltage, while ripple ratio is calculated by percentage of oscillation presented in DC link voltage with respect to settled voltage. PSFC-BC has a ripple ratio of 0.074 %, while ANN-BC has a ripple ratio of 0.017 %, which is less than PSFC-BC. Whereas the ANN-SZSC has a ripple ratio of 0.005%, which is significantly less than the other two controllers. PSFC-BC and ANN-BC have steady-state errors of 1.21 % and 0.51 %, respectively, whereas ANN-SZSC has a steady-state error of -0.11 %. The results indicate that the ANN-SZSC outperforms the PSFC-BC and ANN-BC in all aspects.

Influence of different MPPT methods and two different DC-DC converters in DC bus voltage control is analysed in the aspect of steady state error and settling time. Steady state error is the parameter analysed to know the influence of each configuration by settling value of DC bus voltage. Settling time of DC bus voltage decides the initiative of load/ grid voltage, hence both parameters are compared for performance analysis. Comparative performance of settling time of DC bus voltage of proposed system over existing system is presented in Table 4.

Table 4 Comparison of settling time of DC bus voltage

Control strategies	Settling time (s)
Boost PSFC [16]	>1
SZSC ANN	1.0

From Table 4, it is noted that boost PSFC based DSWIG system by Ayoub Kavousi et al., (2018) [16] revealed that conventional boost converter and PSFC consumes more than 1s for settling DC link voltage. In this article also the same system takes 1.15s for settling DC link voltage, while the proposed MPPT and DC-DC converter reduce it to 1s, which shows that compared to existing system [16] performance of voltage is enriched with the help of proposed system.

6. Conclusion

In this article, dual stator winding induction-generator-based WECS using ANN MPPT is analysed. The DC-DC converter in WECS shows a crucial part in optimising and improving the output power & voltage. In this article, enhancement in WECS using DWIG is analysed using enrichment in the DC-DC converter and MPPT. In this article, a switched Z-source DC/DC converter is proposed for acquiring a high-voltage gain with a minimum duty ratio and a simplified topology to avoid instability. Backpropagation ANN MPPT is implemented for tracking maximum power and regulating the voltage of the DC bus voltage. Three control approaches are analysed in power winding, such as boost converter with PSFC MPPT, boost converter with ANN MPPT and switched Z-source converter with ANN MPPT. The entire system is analysed at various speeds with the ON and OFF states of the converter. The superior performance of the proponed system is authenticated by comparing the performance of three control approaches in terms of DC bus voltage and tracked power with tracking time. The power tracked by the PSFC MPPT is 0.99283 p.u., while it is improved to 0.9999 p.u with the help of ANN MPPT. This analysis shows that ANN improves the performance of power tracking by validating the effectiveness of ANN MPPT. Power quality improvement by the proposed system in the aspect of DC link voltage is validated by reduced steady state error and ripple ratio. The advanced SZSC converter in the proposed WECS using DWIG reduces around 90% of the steady state error and ripple in DC bus voltage compared to the conventional boost converter. Hence, the analysis validates the enriched performance of the proposed system in the aspects of maximum power tracked, tracking time and quality of voltage. In this article, neural network-based MPPT is analysed. In the future, the analysis may be extended to include deep learning or deep neural network, which has many hidden layers and many nodes in every hidden layer. Due to financial limitations, simulation analysis alone is

presented for various topologies. In the future, analysis may extend to hardware implementation.

References

[1] S. Ghoudelbourk, D. Dib, A. Omeiri and AT. Azar, "MPPT control in wind energy conversion systems and the application of fractional control (PIα) in pitch wind turbine", International Journal of Modelling, Identification and Control, vol 26, no. 2, pp. 140-151, January 2016.

[2] M. Allouche, S. Abderrahim, H.B. Zina and M. Chaabane, "A Novel fuzzy Control Strategy for Maximum Power Point Tracking of Wind Energy Conversion System", International Journal of Smart Grid-ijSmartGrid, vol. 3, pp. 120-127, September 2019.

[3] E. Bekiroglu, M.D. Yazar, "Analysis of Grid Connected Wind Power System", 2019 8th International Conference on Renewable Energy Research and Applications (ICRERA), pp. 869-873, 3-6 November 2019.

[4] C.P. Kumar, S. Pragaspathy, V. Karthikeyan and K.N.S Durga Prakash, "Power quality improvement for a hybrid renewable farm using UPQC", In 2021 International Conference on Artificial Intelligence and Smart Systems (ICAIS), pp. 1483-1488. IEEE, 25-27 March 2021.

[5] J. Chhor, P. Tourou and C. Sourkounis, "On advanced control strategies for DFIG-based wind energy conversion systems during voltage unbalance," 2017 IEEE 6th International Conference on Renewable Energy Research and Applications (ICRERA), pp. 331-338, 5-8 November 2017

[6] S. Vadi, F. B. Gürbüz, R. Bayindir and E. Hossain, "Design and Simulation of a Grid Connected Wind Turbine with Permanent Magnet Synchronous Generator", 2020 8th International Conference on Smart Grid (icSmartGrid), pp. 169-175, 17-19 June 2020

[7] Y. Bakou, A. Harrouz, Colak and K. Kayisli, M. Abid and R. Bayindir, "Robust Controller Based on Sliding Mode Technique of DFIG Integrated to Wind Energy System", 2019 7th International Conference on Smart Grid (icSmartGrid), pp. 144-148 9-11, December 2019

[8] G.K. Singh, "Multi-phase induction machine drive research—A survey", Electric Power Systems Research, vol. 61, pp. 139-147, March 2002.

[9] K.K. Mohapatra, R.S. Kanchan, M.R. Baiju, P.N. Tekwaniand, K. Gopakumar, "Independent field-oriented control of two split-phase induction motors from a single six-phase inverter", IEEE Transactions on Industrial Electronics, vol.52, pp. 1372-1382, October 2005.

[10] S. Karugaba, O. Ojo, "A carrier-based PWM modulation technique for balanced and unbalanced reference voltages in multiphase voltage-source inverters", IEEE Transactions on Industry Applications, vol. 48, pp. 2102-2109, Nov-Dec 2012.

[11] K. Shi, W. Huang, Y. Hu and F. Bu, "An indirect-field-oriented dual stator-winding induction generator for the wind power system applications", World Non-Grid-Connected Wind Power and Energy Conference, pp. 1-5. IEEE, September 2009.

[12] K. Shi, P. Xu, Z. Wan, F. Bu, Z. Fang, R. Liu and D. Zhao, "Grid-connected dual stator-winding induction generator wind power system for wide wind speed ranges", Journal of Power Electronics, vol. 16, pp. 1455-1468, July 2016.

[13] M. Benakcha, L. Benalia, F. Ameur and D.E. Tourqui, "Control of dual stator induction generator integrated in wind energy conversion system." Journal of Energy Systems, vol. 1, pp. 21-31, September 2017.

[14] K. Hamitouche, S. Chekkal, H. Amimeur and D. Aouzellag, "A New Control Strategy of Dual Stator Induction Generator with Power Regulation", Journal Européen des Systèmes Automatisés, vol. 53, pp. 469-478, September 2020.

[15] J.I. Talpone, P.F. Puleston, M.G. Cendoya and J. Barrado-Rodrigo, "A dual-stator winding induction generator-based wind-turbine controlled via super-twisting sliding mode", Energies, vol. 12, pp. 4478, November 2019.

[16] A. Kavousi, S. Fathi, J. Milimonfared and M.N. Soltani, "Application of boost converter to increase the speed range of dual-stator winding induction generator in wind power systems", IEEE Transactions on Power Electronics, vol. 33, no. 11, pp. 9599-9610, November 2018.

[17] A. Mustapha, S.K. Selvaperumal H. Mohd and R. Lakshmanan, "Ann-Based Maximum Power Point Tracking of a Variable-Speed Wind Energy Conversion System using Sepic Converter", International Journal of Advanced Science and Technology, vol. 29, pp. 189-205, 2020.

[18] D. Reddyand, S. RamaSwamy "A back propagation network based MPPT algorithm for grid-tied wind energy system with Vienna Rectifier", International Journal of Renewable Energy Research (IJRER), vol. 9, pp. 1097-1107, June 2019.

[19] A. Choudhary, D. Pandey and S. Bhardwaj, "Artificial neural networks based solar radiation estimation using back propagation algorithm", International Journal of Renewable Energy Research (IJRER), vol.10, pp. 1566-1575, December 2020.

[20] K.B. Tawfiq, A.S. Mansour, H.S. Ramadan, M. Becherif and E.E. El-Kholy, "Wind energy conversion system topologies and converters: Comparative review", Energy Procedia, vol. 162, pp. 38-47, April 2019.

[21] P. Krause, O. Wasynczuk, S. Sudhoff and S. Pekarek, "Analysis of Electric Machinery and Drive Systems", 3rd ed., Piscataway, NJ, USA: Wiley-IEEE Press, pp.1-52, 2013.

[22] H. Xu, F. Bu, W. Huang, Y. Hu and H. Liu, “Control and Performance of Five-Phase Dual Stator-Winding Induction Generator DC Generating System”, IEEE Transactions on Industrial Electronics, vol. 64, pp. 5276-85, March 2017.

[23] Y. Li, Y. Hu, W. Huang and L. Liu and Y. Zhang, "The capacity optimization for the static excitation controller of the dual-stator-winding induction generator operating in a wide speed range", IEEE Transactions on Industrial Electronics, vol. 56, pp. 530-541, 2008.

[24] H. Xu, F. Bu, W. Huang, and Y. Hu, H. Liu, and Y. Zhao "Analysis, comparison, and discussion of control strategies for dual stator-winding induction generator DC generating system", IEEE Journal of Emerging and Selected Topics in Power Electronics, vol. 4, pp. 1007-1014, September 2016.

[25] A.S. Yilmaz, Z. Özer, "Pitch angle control in wind turbines above the rated wind speed by multi-layer perceptron and radial basis function neural networks", Expert Systems with Applications, vol. 36, pp. 9767-9775, August 2009.

[26] G. Zhang, H.H. ChingIu, B. Zhang, Z. Li, T. Fernando S.Z. Chen and Y. Zhang, “An impedance network boost converter with a high-voltage gain”, IEEE Transactions on Power Electronics, vol. 32, pp. 6661-6665, September 2017.

[27] X. Fang “A novel Z-source dc-dc converter”, In Proceeding IEEE International Conference on Industrial Technology (ICIT’08), pp. 574-578, 2009.

[28] J. Liu, J. Wu, J. Qiu and J. Zeng “Switched Z-source/quasi-Z-source DC-DC converters with reduced passive components for photovoltaic systems”, IEEE Access, vol.26, pp. 40893-903, March 2019.